

The accretion of brown dwarfs and planets by giant stars – II. Solar-mass stars on the red giant branch

Lionel Siess^{1,2} and Mario Livio¹★

¹Space Telescope Science Institute, 3700 San Martin Drive, Baltimore, MD 21218, USA

²Laboratoire d'Astrophysique de l'Observatoire de Grenoble, Université Joseph Fourier, B.P.53X, F-38041 Grenoble Cedex, France

Accepted 1999 May 10. Received 1999 March 15; in original form 1998 December 3

ABSTRACT

This paper extends our previous study of planet/brown dwarf accretion by giant stars to solar-mass stars located on the red giant branch. The model assumes that the planet is dissipated at the bottom of the convective envelope of the giant star. The evolution of the giant is then followed in detail. We analyse the effects of different accretion rates and different initial conditions. The computations indicate that the accretion process is accompanied by a substantial expansion of the star, and, in the case of high accretion rates, hot bottom burning can be activated. The possible observational signatures that accompany the engulfing of a planet are also extensively investigated. They include the ejection of a shell and a subsequent phase of IR emission, an increase in the ⁷Li surface abundance and a potential stellar metallicity enrichment, spin-up of the star because of the deposition of orbital angular momentum, the possible generation of magnetic fields and the related X-ray activity caused by the development of shear at the base of the convective envelope, and the effects on the morphology of the horizontal branch in globular clusters. We propose that the IR excess and high Li abundance observed in 4–8 per cent of the G and K giants originate from the accretion of a giant planet, a brown dwarf or a very low-mass star.

Key words: accretion, accretion discs – planets and satellites: general – stars: chemically peculiar – stars: evolution – stars: low-mass, brown dwarfs – stars: rotation.

1 INTRODUCTION

Planets and brown dwarfs have now been detected around several main-sequence stars (e.g. Mayor & Queloz 1995; Rebolo, Zapatero-Osorio & Martin 1995; Butler & Marcy 1996; Basri, Marcy & Graham 1996; Rebolo et al. 1996; Cochran et al. 1997; Butler et al. 1998; Delfosse et al. 1998; Marcy et al. 1998) and, strikingly, a fraction of these ‘hot Jupiters’ orbit very close to the central star, at less than 1 AU. This proximity to the central star poses a theoretical problem regarding the mechanism that brought these planets to these orbits, but it also raises the question of their fate. Indeed, Rasio et al. (1996) showed that the orbit of 51 Peg’s companion is tidally unstable, and that the planet will ultimately be engulfed in the stellar envelope. The problem we address here is that of the effects of the accretion of a giant planet or a brown dwarf on the structure and evolution of solar-mass stars on the red giant branch (RGB). This study is the continuation of our previous work (Siess & Livio 1999), in which we investigated the swallowing of massive planets/brown dwarfs by a 3- M_{\odot} AGB star.

The general scenario for the accretion process is as follows:

planets in close orbits (as observed) will be engulfed in the envelope of giant stars as the latter evolve away from the main sequence. Due to viscous and tidal forces, angular momentum is imparted to the envelope and the planet spirals-in. Previous studies of the spiralling-in process (e.g. Livio & Soker 1984; Soker, Harpaz & Livio 1984) have revealed that, depending on the mass of the planet/brown dwarf, three different evolutionary paths can take place. If the mass of the planet is larger than some critical value M_{crit} , the planet can accrete a fraction of the envelope mass. On the other hand, lower mass planets will either evaporate or collide with the stellar core. For the specific stellar model used in their computation, Livio & Soker (1984) estimated $M_{\text{crit}} \sim 20M_{\text{Jup}}$. However, these results must be taken with great caution, since the physical processes were treated only approximatively. We also emphasize that such computations are very sensitive to the stellar model, notably to the size and mass of the convective envelope. More recently, Sandquist et al. (1998) performed 3D hydrodynamical simulations of Jupiter-like planets impacting on to solar-type main-sequence stars. They also found that depending on the initial stellar model, planets can be evaporated or survive the crossing of the convective zone.

The present work has been motivated by the fact that planets

★ E-mail: mlivio@stsci.edu

surrounding low-mass stars are more likely to be engulfed in the star's envelope during the RGB phase than during the asymptotic giant branch (AGB) phase. Indeed, if we compare (for different stars) the ratio of the maximum radius a star can reach during the RGB to its maximum radius on the AGB phase, this ratio is much closer to one for low-mass stars ($M \lesssim 2M_{\odot}$) than for more massive stars (e.g. Soker 1998). Consequently, we expect that in most cases low-mass stars will interact with close low-mass binary companions on the RGB.

In the present paper we used a spherically symmetric stellar evolution code to follow the evolution of a solar-type star that accretes a giant planet or a brown dwarf on the RGB. In Section 2 we describe briefly the computational approach and the initial models. Then, in Section 3, we analyse the effects of accretion on the structure and the evolution of the star. We present results for different mass accretion rates and different initial stellar models on the RGB. The observational signatures expected from this process are investigated in detail in Section 4. A discussion and conclusions follow.

2 INITIAL CONDITIONS

To investigate the effects of planet accretion by solar-type stars, we used three different evolutionary models of the Sun corresponding to three different points on the RGB. These models are characterized by their mass, which is equal to $M = 1.0, 0.9$ and $0.8M_{\odot}$ and they are referred to as models #A, #B and #C, respectively. The main properties of the initial models are summarized in Table 1. The general RGB structure is a degenerate He core, surrounded by a thin hydrogen-burning shell (HBS) that provides most of the luminosity. A thin radiative layer separates the HBS from the large convective envelope. The star was assumed to lose mass as prescribed by Reimer's (1975) law at a rate given by

$$\dot{M}_{\text{loss}} = -3.98 \times 10^{-13} \eta_R \frac{LR}{M} M_{\odot} \text{yr}^{-1}, \quad (1)$$

where the parameter $\eta_R = 0.5$ in our computations, and L, R and M are given in solar units.

The input physics for the accretion process has been previously described by Siess & Livio (1999). Briefly, to determine the locus of the dissipation process, we estimated the virial temperature of the brown dwarf and the critical radius at which tidal effects lead to a total disruption of the brown dwarf. For characteristic values of the mass and radius for the brown dwarf, we found a temperature of a few million K and a critical radius of the order of $\sim 0.1 - 1R_{\odot}$. From the numbers presented in Table 1, we can localize the accretion process at the bottom of the convective envelope near the HBS. To estimate the accretion rate \dot{M}_{acc} , we determined the orbital decay time-scale of the brown dwarf in the vicinity of the dissipation region. This time-scale roughly corresponds to the time required by the brown dwarf to cross the dissipation region, and thus represents the rate at which mass is added there. For typical stellar parameters, we inferred mass accretion rates of the order of $10^{-4} - 10^{-5} M_{\odot} \text{yr}^{-1}$, depending mainly on the mass of the brown dwarf.

During the accretion phase, we adopted a uniform mass deposition profile as described in Siess & Livio (1999). More specifically, we deposit in each numerical shell an amount of accreted matter proportional to the mass of the shell, starting from the top of the HBS and up to a radius $r = 1R_{\odot}$. Our simulations indicate that small changes in the profile of mass deposition do not

Table 1. Physical properties of the initial models.

| | #A | #B | #C |
|--|-----------------------|-----------------------|-----------------------|
| Mass (M_{\odot}) | 0.9928 | 0.9004 | 0.8072 |
| Radius (R_{\odot}) | 10.72 | 88.71 | 137.10 |
| L (L_{\odot}) | 45.2 | 1133.6 | 2016.3 |
| age t_0 (10^9 yr) | 12.1398325 | 12.1999969 | 12.2022346 |
| k_{env}^{\dagger} | 0.3324 | 0.2366 | 0.2098 |
| $M_{\text{env,bot}}$ (M_{\odot}) | 0.2583 | 0.3904 | 0.4336 |
| $M_{\text{HBS,top}}$ (M_{\odot}) | 0.2474 | 0.3883 | 0.4322 |
| M_{core} (M_{\odot}) | 0.2419 | 0.3867 | 0.4310 |
| $R_{\text{env,bot}}$ (R_{\odot}) | 0.543 | 0.791 | 0.831 |
| $R_{\text{HBS,top}}$ (R_{\odot}) | 0.08586 | 0.1033 | 0.1060 |
| R_{core} (R_{\odot}) | 0.02587 | 0.02538 | 0.02492 |
| $\rho_{\text{env,bot}}$ (g cm^{-3}) | $4.057 \cdot 10^{-2}$ | $1.586 \cdot 10^{-3}$ | $8.715 \cdot 10^{-4}$ |
| $\rho_{\text{HBS,top}}$ (g cm^{-3}) | 2.733 | 0.3726 | 0.2510 |
| ρ_{core} (g cm^{-3}) | 369.7 | 135.2 | 112.0 |
| $T_{\text{env,bot}}$ (10^6 K) | 3.286 | 2.324 | 2.209 |
| $T_{\text{HBS,top}}$ (10^6 K) | 11.0 | 12.3 | 12.6 |
| T_{core} (10^6 K) | 29.8 | 44.5 | 48.2 |
| T_c (10^6 K) ‡ | 34.6 | 60.9 | 69.9 |

† gyration radius [$(I_{\text{env}}/M_{\text{env}}R_{\text{env}}^2)^{1/2}$].

‡ central temperature.

substantially affect the results. The main point here is the depth at which the mass is deposited inside the star, and in the following sections we identify the *accretion zone* as the region located close to the base of the convective envelope where most of the energy accompanying the accretion process is released. Finally, if the convective envelope reaches the HBS (beginning of hot bottom burning, or HBB), the matter is deposited from the base of the convective envelope (which is inside the HBS). In our computations, we also assumed that the matter is deposited with the same entropy as the one of the local matter, implying that the rotational energy has been used to heat up the accreted matter (e.g. Harpaz & Soker 1994). The deposition of accreted matter is also accompanied by modifications of the chemical abundances. We adopted a solar metallicity with relative abundances given by Anders & Grevesse (1989) for the accreted matter, and we assumed that deuterium had been previously burnt in the brown dwarf. Finally, for numerical convenience, we turned off the mass-loss during the accretion phase and used grey atmosphere models to speed up the convergence process.

3 NUMERICAL RESULTS

The stellar evolutionary code used in these computations has been described in detail in several papers (e.g. Forestini & Charbonnel 1997; Siess, Forestini & Bertout 1997), and we refer the reader to those publications for more details. Computations are presented for two characteristic accretion rates of 10^{-4} and $10^{-5} M_{\odot} \text{yr}^{-1}$, and they involve different masses for the planet/brown dwarf (see Table 2).

3.1 Evolution of the structure for lower accretion rates

The deposition of mass in the star is accompanied by the release of a large amount of gravitational energy that acts to expand the envelope (Fig. 1). However, because of the long time-scale of heat diffusion, the expansion is delayed, especially for the low-luminosity stars (cases A0 and A1). As the radius increases, the star also becomes more luminous. According to Reimer's law, these modifications to the structure significantly increase the mass-loss rate, and we expect some changes in the subsequent

evolution and stellar environment (see Sections 4.4 and 4.5). The expansion proceeds until a thermal equilibrium is reached, in which the rate of energy loss by the surface balances the rate of energy deposition by the accretion process. Depending on the initial model, the return to contraction occurs after ~ 6200 , ~ 470 and ~ 200 yr, in cases A0, B0 and C0, respectively. This time-scale corresponds roughly to the time of heat diffusion (thermal time-scale) of the expanding part of the star, and it is approximately given by $\tau_{\text{therm}} \sim \mathcal{G} M M_{\text{env}} / 2 R L_{\text{acc}}$, where M_{env}

is the mass of the envelope, and L_{acc} is the accretion luminosity. The latter is given by $L_{\text{acc}}(r) = \mathcal{G} M_r \dot{M}_{\text{acc}} / r$, where \dot{M}_{acc} is the mass accretion rate, and M_r and r are the mass and radial coordinates of the accretion zone. It should be noted that L_{acc} represents an upper limit to the accretion luminosity, since energy is lost during the spiralling-in process to heating and spinning up the envelope. However, throughout most of the envelope, the orbital energy dissipation rate represents a small fraction of the intrinsic stellar luminosity, and thus we do not expect that the stellar structure will be significantly affected until the planet reaches the accretion zone. Finally, we should mention that the energy deposition might not be local (in the accretion region). For example, the star could be tidally excited, oscillations may be initiated and then damped elsewhere in the envelope. Also, in this common-envelope phase, magnetic fields might be generated in the accretion region (see Section 4.3) and energy could be dissipated at the surface of the star or in the corona (e.g. Regos & Tout 1995).

During the envelope expansion, the opacity κ increases in the accretion region, and rapidly the radiative gradient becomes larger than the adiabatic one ($\nabla_{\text{rad}} \propto \kappa L > \nabla_{\text{ad}}$); thus the convective envelope deepens (Fig. 2). Thereafter, as the HBS advances in mass and reaches the cool regions that have been previously expanded, the nuclear energy production rate decreases significantly. As an order of magnitude, during most of the accretion phase, the luminosity due to H burning represents only a few per cent of the total stellar luminosity. The accretion luminosity thus

Table 2. Numerical models.

| Models | $M_{\text{ini}} (M_{\odot})$ | $\dot{M}_{\text{acc}} (M_{\odot} \text{yr}^{-1})$ | accreted mass (M_{\odot}) |
|-----------------|------------------------------|---|-------------------------------|
| A0 | 0.99 | 10^{-5} | 0.10 |
| A1 | 0.99 | 10^{-5} | 0.01 |
| A2 | 0.99 | 10^{-4} | 0.10 |
| A3 | 0.99 | 10^{-4} | 0.01 |
| B0 | 0.90 | 10^{-5} | 0.10 |
| B1 | 0.90 | 10^{-5} | 0.01 |
| B2 | 0.90 | 10^{-4} | 0.0051 |
| B3 [†] | 0.90 | 10^{-4} | 0.0058 |
| C0 | 0.81 | 10^{-5} | 0.10 |
| C1 | 0.81 | 10^{-5} | 0.01 |
| C2 | 0.81 | 10^{-4} | 0.0010 |
| C3 | 0.81 | 10^{-4} | 0.0025 |
| C4 [†] | 0.81 | 10^{-4} | 0.0030 |

[†]For these models, we were not able to follow reliably the evolution, and the computations were stopped at the indicated accreted mass.

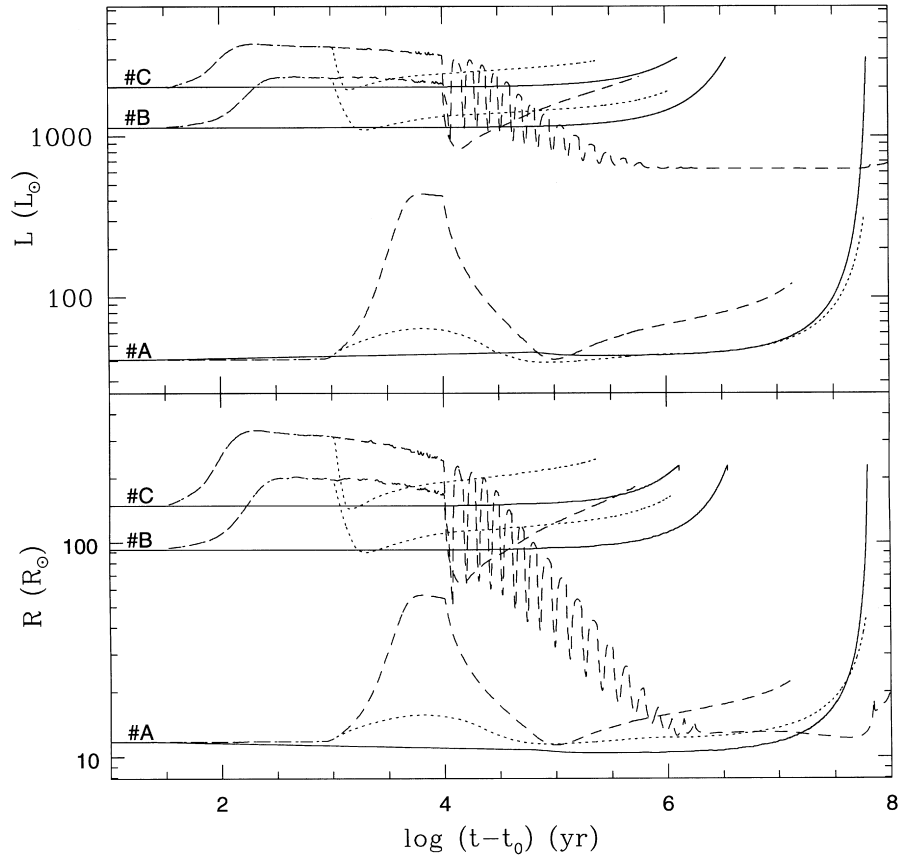


Figure 1. The evolution of the radius R and luminosity L for the different models computed with a lower accretion rate ($\dot{M}_{\text{acc}} = 10^{-5} M_{\odot} \text{yr}^{-1}$). The time t_0 corresponds to the age of the initial model, and is indicated for the different models in Table 1. The solid lines refer to the standard solar model (no accretion), and the dotted and dashed lines correspond to models in which the accreted mass is equal to 0.01 and $0.1 M_{\odot}$, respectively. The depicted models are A0, A1, B0, B1, C0 and C1.

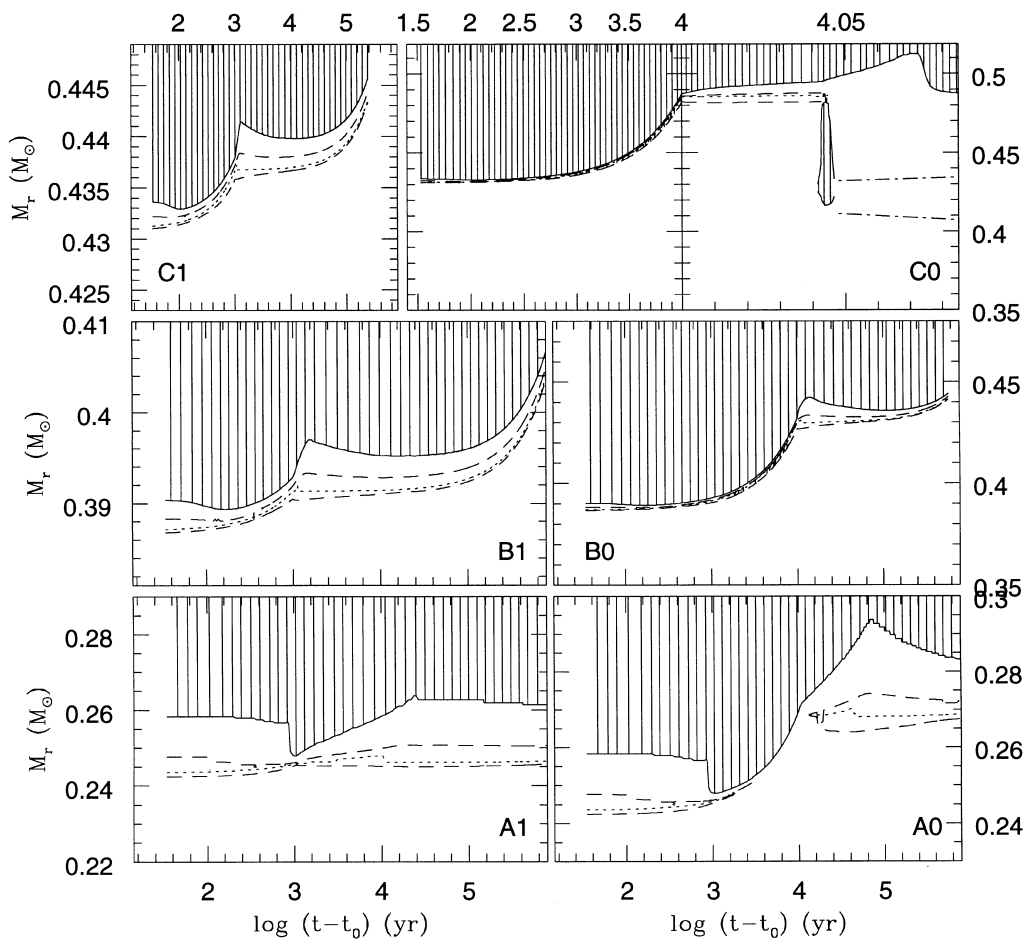


Figure 2. The evolution of the boundaries of the HBS and the convective envelope. The dashed lines delineate the burning shells ($\epsilon_{\text{nuc}} > 5 \text{ erg g}^{-1} \text{ s}^{-1}$), and the dotted line indicates the locus of maximum energy generation. The hatched areas indicate convective regions. The different models are labelled in each panel and were computed with an accretion rate equal to $10^{-5} M_\odot \text{ yr}^{-1}$. Note the extinction of the HBS in case A0 (lower right panel). In the upper right panel (case C0), a thermal instability develops and leads to the development of a convective tongue. The dot-dashed lines delineate the He-burning shell.

supports the convective envelope almost entirely, and the accretion region acts as a source shell that prevents an efficient H burning.

To see how the structure is affected by the accretion process, we have presented in Fig. 3 the profiles of several variables for case A0, but they are globally similar in the other models. In the accretion region where a large amount of energy is deposited, the luminosity and temperature rise. However, due to the relatively long time-scale associated with heat diffusion, energy accumulates locally and both profiles now present a bump. The heat excess finally diffuses when the star has sufficiently expanded, and a monotonically increasing luminosity profile is restored. However, the temperature profile still presents a local maximum that persists throughout the accretion phase. This is due to the fact that this region undergoes a compressional heating from the mass accumulated above it, and also from the expanding region surrounding the core. Indeed, the luminosity L_r is negative just behind the luminosity jump, indicating a region in expansion ($\epsilon_{\text{grav}} < 0$). The temperature is thus compelled to rise and, as we shall see in Section 3.3, this situation can give rise to a thermal instability. The temperature gradient also becomes progressively steeper beyond the bump (Fig. 3) as energy accumulates. This contributes to the shrinkage of the HBS and to the subsequent drop in the nuclear luminosity.

In the HBS, prior to accretion, the nuclear energy production rate is mainly supplied by the CNO bi-cycle. More precisely, the most important reactions (and their contribution) are $^{13}\text{C}(p,\gamma)^{14}\text{N}$ (~ 25 per cent), $^{14}\text{N}(p,\gamma)^{15}\text{O}$ (~ 23 per cent), $^{15}\text{N}(p,\alpha)^{12}\text{C}$ (~ 16 per cent) and $^{15}\text{O}(\beta^+, \nu)^{15}\text{N}$ (~ 16 per cent). However, because the HBS advances in mass into a cooler region, the pp1 branch progressively takes over the nuclear energy production, and during the accretion phase the reactions $2\ ^3\text{He}(\gamma,2p)\alpha$ and $^{13}\text{C}(p,\gamma)^{14}\text{N}$ contribute ~ 45 and ~ 10 per cent of the total nuclear energy production, respectively. On the other hand, in the region of maximum temperature, ^{13}C is now efficiently burnt through the $^{13}\text{C}(\alpha,n)^{16}\text{O}$ reaction. This reaction is highly energetic and provides up to ~ 20 per cent of the global nuclear energy production (which still remains very low, however). In Fig. 4 we show the evolution of the nuclear activity for case B0. First, ^{13}C burning is ignited in the vicinity of the temperature peak (dotted line). Then, as it is depleted and converted into ^{16}O , the nuclear energy production rate progressively decreases near the temperature peak (short-dashed and long-dashed curves), and finally we end up with a configuration in which ^{13}C is burnt through $^{13}\text{C}(\alpha,n)^{16}\text{O}$ around the temperature peak and through $^{13}\text{C}(p,\gamma)^{14}\text{N}$ above the bump in the HBS. In case C0, the temperature in the peak reaches $\sim 1.2 \times 10^8 \text{ K}$ and He is ignited

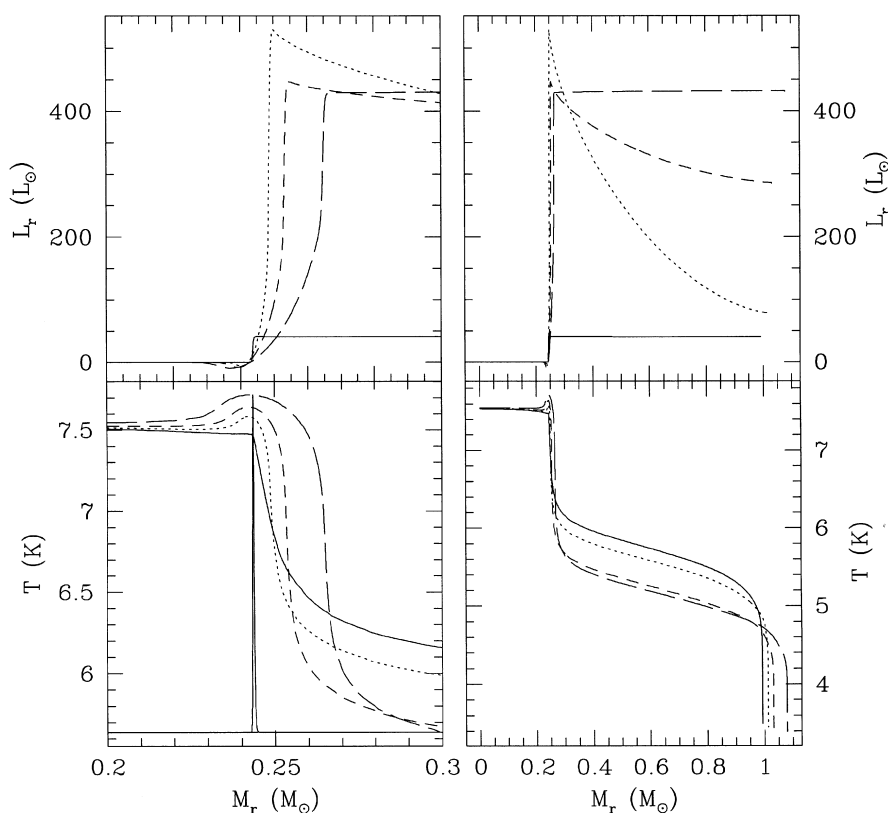


Figure 3. The evolution of the profiles of luminosity (L_r) and temperature (T) for case A0. The solid line refers to the initial model, and the dotted, short-dashed and long-dashed lines correspond to models for which 0.019 , 0.039 and $0.086 M_{\odot}$ have been accreted, respectively. The accretion rate is equal to $10^{-5} M_{\odot} \text{yr}^{-1}$. The peak in the lower left panel represents the nuclear energy production rate in the initial model, and thus delineates the H-burning shell.

off-centre in a non-degenerate shell (we will discuss this special case further in Section 3.3).

3.2 Higher accretion rates

For higher accretion rates, the situation is somewhat different because of the appearance of hot bottom burning (HBB). Indeed, contrary to the lower accretion rate case, the larger energy release contributes to a further increase in the opacity and the convective envelope deepens even more. It finally reaches the HBS where its advance stops (Fig. 5). Our computations indicate that HBB is activated approximately 200, 25 and 15 yr after the onset of accretion in cases A2, B2 and C2, respectively. The temperature at the base of the convective envelope rises suddenly from ~ 2 – 3 to about 13 – 18 million Kelvin, depending on the initial model. However, this temperature is still too low to give rise to a rich nucleosynthesis. The onset of HBB entails a significant and fast expansion of the envelope as heat is directly transferred to the convective zone. Moreover, the arrival of ${}^3\text{He}$ from the convective envelope and its destruction through the reaction $2 {}^3\text{He}(\gamma, 2p)\alpha$ increase temporarily the nuclear luminosity in the HBS. During the HBB phase, ${}^7\text{Li}$ is slowly depleted because of the competing effects of Li production through the reactions $\alpha({}^3\text{He}, \gamma){}^7\text{Be}(e^-, \nu){}^7\text{Li}$ and Li destruction through the reaction ${}^7\text{Li}(p, \alpha)\alpha$ (see also Section 4.1).

Finally, in cases B2 and C2 we were not able to follow reliably the computations. The star’s tendency to expand and increase its luminosity made the computations intractable. At that point the

envelope is probably ejected and the star enters a protoplanetary nebula phase.

3.3 The relaxation of the star

After the end of the accretion phase, the envelope rapidly contracts because of the sudden suppression of accretion energy. However, in the models in which the duration of the accretion process is shorter than the thermal time-scale associated with the envelope (as in cases B1 and C1 for example), the expansion still proceeds for a while after the end of mass addition. Thereafter, the gravitational energy released during the contraction phase heats up the central parts of the star and the HBS re-ignites. During that period of contraction, the convective envelope retreats towards the surface, and HBB disappears. The contraction rate is very fast, especially for stars having a shallower convective envelope. The computations indicate that in a few thousand years, the radius decreases by a factor of ~ 2 – 3 which, we suspect, could initiate stellar pulsations. When the HBS finally provides most of the stellar luminosity (≥ 80 per cent), the contraction ends and the star resumes a standard evolution, climbing the RGB until He flashes at its tip. Interestingly, the star is now more luminous and has a larger radius than in the standard evolution, despite the small amount of added mass (Fig. 1). The enhanced mass-loss rate that follows can affect the subsequent evolution (see Section 4.5).

In all our simulations, except for case C0, the temperature ‘bump’ dissipated as the gravitational energy released during the contraction phase heated up the stellar interior. However, in this

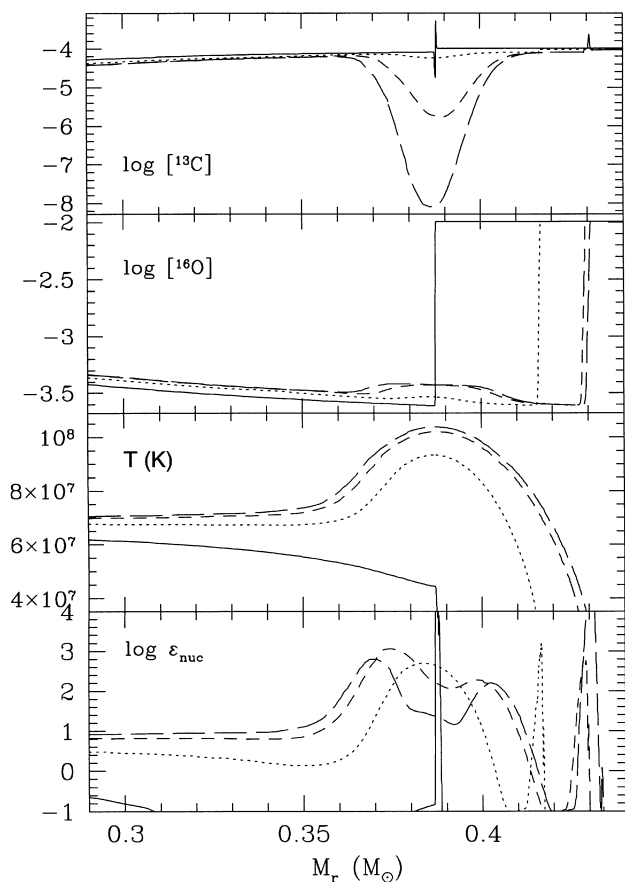


Figure 4. Evolution of the nuclear energy production rate (ϵ_{nuc}), temperature (T), and ^{16}O and ^{13}C chemical abundances for model B0 ($\dot{M}_{\text{acc}} = 10^{-5} M_{\odot} \text{yr}^{-1}$). The solid lines refer to the initial model $t = t_0$. The dotted, short-dashed and long-dashed lines correspond to an age $t - t_0$ equal to 6791, 9760 and 11 040 yr, respectively. Note the persistence of the temperature excess during the accretion phase.

particular model, in which the accretion process is maintained for $\sim 10^4$ yr at a rate equal to $10^{-5} M_{\odot} \text{yr}^{-1}$, the temperature in the peak reaches $\sim 1.2 \times 10^8$ K, and He ignites off-centre in a non-degenerate shell. The ignition of He through the 3α reactions is very energetic, and this gives rise to a thermal instability (Fig. 6). The geometrical thinness and the large opacity of the He-burning shell (HeBS) are responsible for the thermal runaway that leads to the development of a convective tongue. The release of energy due to He burning is used to expand the layers above, and secondarily to heat up the core. The HBS is pushed outward into a cooler region and it extinguishes. The remaining energy excess is then absorbed by the envelope which subsequently expands. During the thermal pulse, the nuclear energy production comes from 3α (~ 70 per cent), $^{14}\text{N}(\alpha, \gamma)^{18}\text{F}$ (~ 17 per cent) and, to a lesser extent, from $^{18}\text{O}(\alpha, \gamma)^{22}\text{Ne}$ and $^{18}\text{O}(\alpha, \gamma)^{22}\text{N}$ (~ 7 per cent each). The thermal pulse is also responsible for the further destruction of H through $^{12}\text{C}(\text{p}, \gamma)^{13}\text{N}$. After a significant expansion that allows the star to get rid of the energy excess, contraction resumes. However, due to the extremely low H content left after the pulse (the H mass fraction $X < 10^{-20}$), the HBS cannot ignite before a new thermal instability is triggered. A new He shell flash thus occurs deeper inside the star where both the temperature and He abundance are higher. As evolution proceeds, the pulse duration increases, but the maximum luminosity due to He burning decreases, mainly

because of the progressive lifting of the core degeneracy as the temperature increases. During the subsequent evolution, the star experiences relatively short phases of expansion following the thermal pulses and longer phases of contraction. The deepening of the pulse accounts for the smaller and smaller increase in radius following the He shell flashes, since most of the released energy is absorbed in the radiative layers before reaching the convective envelope. After the 12th pulse, the HBS ignites precisely at the mass coordinate corresponding to the top of the first convective tongue in which the H abundance is high ($X \gg 10^{-20}$). The H luminosity then increases, and the thermal pulse finally reaches the centre of the star. Because of the previous thermal instabilities, the degeneracy has been lifted in the interior, and consequently He does not flash. Helium is now burnt at the centre, and the star will spend the next $\sim 4 \times 10^7$ yr on the horizontal branch.

4 POTENTIAL OBSERVATIONAL SIGNATURES OF AN ACCRETION EVENT

In this section we attempt to give a broad overview of the different observational signatures that might be expected from the accretion of a planet or a brown dwarf by a giant star on the red giant branch. In general, effects may be expected in at least six different areas, which we describe in some detail below. The modifications to the structure during the accretion process increase the mass-loss rate and may lead to the ejection of shells. They also have potential effects on the morphology of the horizontal branch. The deposition of angular momentum during the spiralling-in process can also alter the stellar structure by increasing the rotation rate, and this may also produce X-ray emission. Finally, the mixing of the dissipated planet material in the envelope can change the surface chemical abundances. All of these effects may have important observational consequences but, as we shall see in the following sections, it is more the combination of several signatures, such as a high rotation rate and/or a large IR excess and/or a high lithium abundance that can identify an accretion event less ambiguously, rather than the detection of one particular signature.

4.1 Modifications of the photospheric chemical composition

During the red giant phase, chemical changes are mainly the result of ‘dilution’ effects due to the deepening of the convective envelope, but light elements such as ^7Li , ^9Be and ^{11}B can also be burnt as the convective envelope approaches its deepest extent. The first dredge-up reduces the ^7Li abundance by more than 2 orders of magnitude. There is also a decrease in the $^{12}\text{C}/^{13}\text{C}$ ratio by a factor of 3, changing from about 83 to 26. The first dredge-up also accounts for the large enrichment of ^3He as a by product of H burning.

With our assumed chemical composition for giant planets and brown dwarfs (from Anders & Grevesse 1989), the deposition of accreted matter, mostly in the convective envelope, will principally modify the chemical abundances of the light elements that were previously depleted during the first dredge-up. In that respect, ^7Li will be the most affected. Our computations indicate that, depending on the accreted mass, the ^7Li abundance can be increased by more than 2 orders of magnitude, making this element easily detectable at the surface of the star¹ (see also Section 4.6). As an illustration, we present in Fig. 7 the ^7Li surface

¹ Following de la Reza, Drake & da Silva (1996), we define as a ‘Li-rich G or K giant’ a star with a Li abundance larger than $\log \epsilon(\text{Li}) = 1.2$ [where, by definition, $\log \epsilon(\text{H}) = 12.00$].

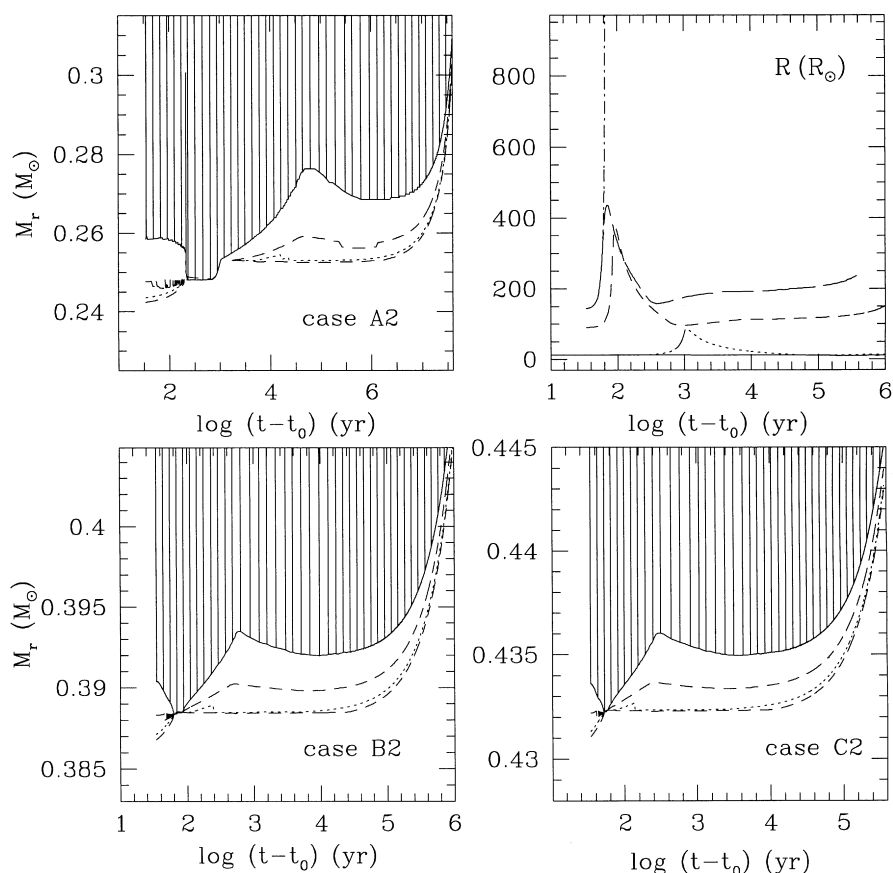


Figure 5. The evolution of the internal structure (left and lower right panels) and radius (upper right panel) for the high accretion rate case ($\dot{M}_{\text{acc}} = 10^{-4} M_\odot \text{yr}^{-1}$). The evolution of the structure is depicted in a similar way to that in Fig. 2. Note the appearance of hot bottom burning in these computations. In the upper right panel, the solid, dotted, short-, long- and dot-dashed lines refer to the standard case and to cases A2, B2, C2 and C4, respectively.

abundances resulting from our computations, and compare them with what is expected from simple dilution effects. In the dilution hypothesis, we assume that the envelope mass M_{env} is held constant during the accretion process, and that no nuclear burning is taking place in the convective zone. The mass fraction X_i of an element i is then simply given by

$$X_i = \frac{X_i^{\text{env}} \times M_{\text{env}} + X_i^{\text{acc}} \times M_{\text{acc}}}{M_{\text{acc}} + M_{\text{env}}}, \quad (2)$$

where M_{acc} is the mass accreted into the envelope, and X_i^{env} and X_i^{acc} are the mass fraction of element i in the envelope and in the accreted matter, respectively. Note that this expression is general in the sense that X_i can either represent the H mass fraction X , the He mass fraction Y or the metallicity Z . Fig. 7 shows that the simulations follow relatively well the theoretical curves defined by equation (2). The slight deviations from this relation are mainly due to nuclear burning that causes Li depletion. Note that in case A2, ${}^7\text{Li}$ is severely depleted due to the long-lasting HBB. The deposition of accreted matter will also increase the ${}^9\text{Be}$ and ${}^{11}\text{B}$ chemical abundances, but to a lower extent, since the effects of dilution during the first dredge-up are smaller for these elements. A modest increase in the ${}^{12}\text{C}/{}^{13}\text{C}$ ratio can also take place.

The effects of planet accretion on the stellar metallicity are very sensitive to the amount and chemical composition of the accreted material, and also to the mass of the convective envelope (which depends on the evolutionary status of the star). If the metal content

of the giant planet is higher than the one adopted here, the metallicity can be further enhanced. Secondly, if the planet is engulfed while the star is still on the main sequence for example, the convective envelope is then very shallow ($M_{\text{env}} \approx 0.02 M_\odot$ for the Sun), and consequently the stellar photospheric composition can be substantially modified (equation 2). Recent determinations of the chemical composition of the main-sequence stars hosting planets (Gonzales 1997, 1998) indeed show that in some cases the metallicity is abnormally high, suggesting that protoplanetary material or planets have been accreted (e.g. Lin, Bodenheimer & Richardson 1996; Laughlin & Adams 1997). More recently, Sandquist et al. (1998) showed that a Jupiter-like planet can be evaporated in the convective envelope of the Sun. They also inferred that in some cases a metal enrichment as high as 50 per cent can be obtained, but the exact value depends greatly on the mass of the convective zone and on the chemical composition and interior structure of the giant planet.

All the above suggests that if the presence of planets around solar-type stars is rather common, and if some of these planets are indeed in close orbits, then certain chemical peculiarities in giants stars may be the consequence of the accretion of planets.

4.2 Rotation

During the spiralling-in process, angular momentum is imparted to the envelope. As a consequence, the stellar rotation rate will be

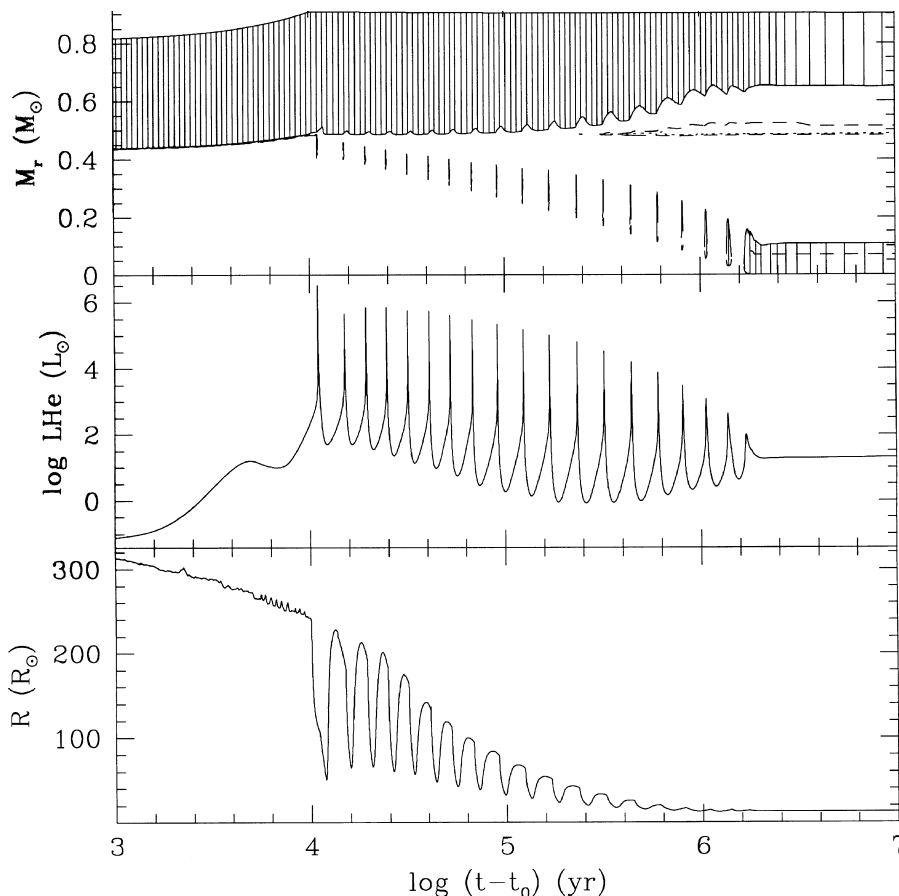


Figure 6. The evolution of the radius, He luminosity and internal structure for case C0. In the upper panel, the different lines follow the same convention as in Fig. 2.

substantially increased. More quantitatively, if all the orbital angular momentum of the planet is entirely deposited and redistributed in the envelope, i.e., if we assume that the convective envelope is rotating rigidly, then the ratio of the envelope angular velocity ω to the critical velocity (surface Keplerian angular velocity) ω_K is given by

$$\frac{\omega}{\omega_K} \approx 0.10 \left(\frac{M_{\text{bd}}}{0.01 M_{\odot}} \right) \left(\frac{M_{\text{env}}}{M_{\odot}} \right)^{-1} \left(\frac{k^2}{0.1} \right)^{-1} \left(\frac{a}{R} \right)^{1/2}, \quad (3)$$

where a is the orbital separation of the brown dwarf, k the gyration radius, and M_{env} the mass of the envelope. Equation (3) indicates that only massive planets or brown dwarfs ($M_{\text{bd}} > 5M_{\text{Jup}}$) can spin-up the giant envelope to a significant fraction of the Keplerian velocity (≈ 10 per cent). The spin-up would be most effective at the tip of the giant branch, where both M_{env} and k are smaller.

Measurements of the projected rotational velocity of luminous class III giants indicate a sudden drop in $v \sin i$ near spectral type G0III (Gray 1989). The same discontinuity is also observed in subgiants at spectral type F8IV (Gray & Nagar 1985) and on the main sequence near mid-F stars (Kraft 1970). These observations thus delineate in the HR diagram a rotational dividing line (RDL) where slow rotators ($v \sin i \lesssim 5 \text{ km s}^{-1}$) populate the cool side (de Medeiros, da Rocha & Mayor 1996b). The strong braking at the rotational discontinuity occurs very rapidly, perhaps on a time-scale as short as $\sim 10^5$ yr or less (Ayres et al. 1998), and probably results from an efficient magnetic braking attributed to a dynamo

action (Gray 1981, 1982). In the ‘rotostat’ hypothesis (Gray 1986), angular momentum is dredged up from the rapidly rotating core by the deepening of the convective envelope. This activates the dynamo and then an efficient magnetic braking takes place. In this model, the rotation rate is controlled in a self-regulatory way by the balance between the arrival of angular momentum from the core and the strong braking that ensues, and consequently the rotational velocity is maintained constant. However, a few stars do not conform to this scheme and still rotate rapidly beyond the RDL, challenging the rotostat hypothesis. For example, the case of 7 Boo = HR 5225 remains unexplained (Gray 1989, 1991). This single star of spectral type G5III has a moderate lithium abundance $\log \epsilon(\text{Li}) = 1.2$, and its rotational velocity ($v \sin i = 14.1 \text{ km s}^{-1}$) is 3 times higher than the average. This isolated case could fit into a scenario in which the giant star has recently accreted a planet and its surface layers have not yet spun down. The moderate lithium abundance would suggest the accretion of a relatively small planet. More generally, de Medeiros, Melo & Mayor (1996a) found that among a sample of ~ 900 stars, less than ~ 5 per cent of the late G and K giants located to the right of the RDL have $v \sin i > 5 \text{ km s}^{-1}$.

On the other side (left) of the RDL, FK Comae-type stars show extreme rotation velocities ($\omega/\omega_K \approx 0.10$). The general explanation for their fast rotation assumes that these single G or K giants are undergoing (or have just completed) coalescence with a close binary companion (e.g. Webbink 1977; Bopp & Stencel 1981; Livio & Soker 1988; Welty and Ramsey 1994). Other scenarios

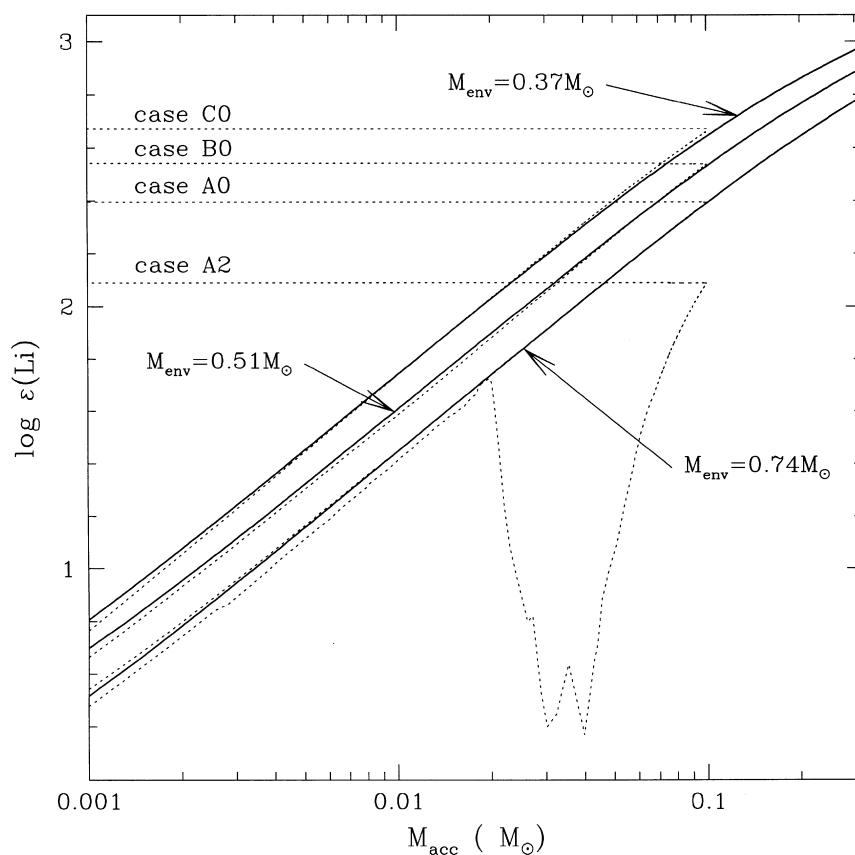


Figure 7. The evolution of the ${}^7\text{Li}$ surface abundance as a function of the accreted mass. The solid lines represent the ${}^7\text{Li}$ abundance as a result of dilution for the three initial envelope masses characterizing our initial models ($M_{\text{env}} = 0.74, 0.51$ and $0.37 M_{\odot}$ in models A, B and C, respectively). The dotted lines represent the results of our computations for cases A0, B0, C0 and A2. Note the large Li depletion in case A2 due to the long-lasting HBB.

have also been proposed and they generally invoke tidal synchronization in a very close binary, normal evolution from a rapidly rotating upper main-sequence star, or the dredge-up of angular momentum (e.g. Simon & Drake 1989). However, as pointed out by Rucinski (1990), FK Coma has a few times more (> 8) angular momentum than a typical rapidly rotating main-sequence star. Therefore some angular momentum must have been added (accreted) to the star. Generally, FK Comae-like stars lack photospheric lithium detection. However, in some cases, e.g., HD 36705 (Rucinski 1985), HD 33798 (Fekel & Marschall 1991) or IE 1751+7046 (Ambruster et al. 1997), a high lithium abundance has been observed (see also Section 4.6). These observations clearly support our accretion scenario, since they combine two different outcomes of the accretion process: a high rotation rate and a high Li abundance. However, different scenarios have also been proposed, among them the possibility that these stars were initially fast rotating A- or F-type stars that have rapidly evolved in the Hertzsprung gap. The suggestion is then that they recently became giants, and are now depleting lithium due to the deepening of the convective envelope (Fekel 1988). It has also been suggested (Fekel & Marschall 1991) that angular momentum and CNO processed material can be dredged up from a rapidly rotating core as the convective zone deepens. In this scenario Li can be produced and burnt through the chain ${}^3\text{He}(\alpha, \gamma){}^7\text{Be}(e, \nu){}^7\text{Li}(p, \alpha){}^4\text{He}$ and, if on its way to the surface Li is not entirely depleted, then we may account for temporarily high rotation together with enhanced lithium abundance. However, this hypothesis would imply that essentially every star arriving to

the RGB should go through a phase of fast rotation and high Li abundance. The paucity of such candidates poses a severe problem to this scenario and can be regarded as additional evidence against the rotostat hypothesis.

To conclude this section, we feel that observations support the coalescence hypothesis for the explanation of FK Comae-like stars, and we stress that rapidly rotating stars may also have accreted angular momentum from the swallowing of a giant planet or a brown dwarf (see also Vitenbroek, Dupree & Gilliland 1998). The planet accretion scenario can also account for enhanced Li abundances, and in that respect HD 33798 and 36705 are good candidates for such an event. Finally, we would like to point out that fast rotation velocities, of the order of $15\text{--}40 \text{ km s}^{-1}$, have also been observed in horizontal branch stars (e.g. Peterson, Rood & Crocker 1995; Cohen & McCarthy 1997). Notably, Peterson, Tarbell & Carney (1983) already mentioned that the deposition, during the red giant phase, of the orbital angular momentum of a planet of a few Jupiter masses could account for the fast rotational velocities observed in horizontal branch stars. Some AGB stars also exhibit high rotation rates (e.g., V Hydrae). For these exceptional stars, the rapid rotation rate is thought to be due to spinning up by a companion that has been swallowed or is in a common-envelope phase (Barnbaum, Morris & Kahane 1995). More generally, the deposition of angular momentum in the envelope of evolved stars by a companion (even substellar) is frequently invoked to explain the axisymmetrical morphology of bipolar nebulae (e.g. Iben & Livio 1993; Livio 1997).

4.3 X-ray emission

If the accretion of angular momentum can cause the star to rotate differentially, then differential rotation and convection can generate a magnetic dynamo. The magnetic field can then confine the plasma in the stellar chromosphere and produce X-ray emission activity. To see if this scenario is plausible, let us first examine the observational situation.

Observations indicate the existence of an X-ray dividing line in the HR diagram (XDL, also called coronal dividing line) which delimits giant stars with (to the left) and without coronal emission characteristic of high-temperature gas ($T > 10^6$ K). In the HR diagram, this line is approximately vertical at spectral type \sim K3, and it spans the luminosity classes II, III and IV (Haisch, Schmitt & Rosso 1991; Haisch, Schmitt & Fabian 1992). Note that bright giants of luminosity class II and Ib turn out to be X-ray sources if exposed sufficiently deeply (Reimers et al. 1996). On the right side of the XDL, the vast majority of the stars exhibit a very low X-ray emission (at least below the actual detection threshold), whereas a large spread of X-ray luminosities is observed for G and K giants of spectral types earlier than K3 (Strassmeier et al. 1994; Hünsch et al. 1996). The X-ray emission originates from the stellar corona and requires a strong magnetic field in order to confine the hot plasma, since the thermal velocity of the particles exceeds the escape velocity. Changes in the magnetic field configuration (due to changes in the dynamo) are generally invoked to account for the sudden drop in X-ray emission at the XDL (e.g. Rosner et al. 1991, 1995), but the precise reasons why the dynamo is modified remain unclear. Recently, Hünsch & Schröder (1996) presented a ‘revised’ XDL that seems to follow the evolutionary track of a $1.2-M_{\odot}$ star. If this is confirmed, then evolutionary effects may account for this demarcation line. Low-mass stars, on the right of the XDL, are generally slow rotators on the main sequence, and consequently they sustain a lower magnetic activity. Conversely, more massive stars ($M \gtrsim 1.6 M_{\odot}$) have faster rotation rates on the main sequence, and therefore they can develop an efficient dynamo and produce a higher X-ray emission. More recently, Hünsch et al. (1998) looked for X-ray emission in the ‘forbidden’ region beyond the XDL, and they detected four intrinsically X-ray-bright M-type giants: 15 Tri, HR 5512, 42 Her and HR 7547. No evidence for binarity exists yet for 15 Tri and HR 5512, but even if the presence of a companion is confirmed, it cannot easily explain the X-ray emission which remains quite unusual.² In a *ROSAT* survey of a complete, volume-limited sample of late-type stars, Hünsch et al. (1996) also pointed out the unusual behaviour of δ Sgr = HR 6859, an apparently single, slowly rotating but strong X-ray-emitting K3III giant. Another puzzling case is that of HR 1362 (Strassmeier et al. 1990). Despite its low rotation rate, this single G8IV giant presents an X-ray emission that is more than one order of magnitude higher than that expected from the empirical rotation versus activity trend. The strong emission of HR 1362 led Stepien (1993) to suggest that it might represent an evolved Ap star that has preserved its strong magnetic field. On the other side (left) of the XDL, several unusually bright X-ray sources have also been detected. They are often referred to as β Ceti-like stars, based on the prototype β Ceti (Hünsch et al. 1996; Maggio et al. 1998),

² A compact companion such as a white dwarf can be a relatively strong X-ray source if it accretes matter from the giant through an accretion disc. However, such a companion would have been detected in their observations.

which exhibits an extremely high X-ray luminosity and a slow rotation rate ($v \sin i \approx 3 \text{ km s}^{-1}$). These observations are puzzling, since it is difficult to reconcile the high X-ray emission with the slow rotation rate. Below we investigate the physical effects related to the accretion of a planet/brown dwarf in terms of the generation of magnetic field and X-ray emission.

Suppose that an initially slowly rotating star undergoes an accretion event. As the planet spirals in, it will deposit angular momentum in the envelope and finally dissipate close to the core. However, the resultant profile of angular velocity $\omega(r)$ may not be uniform throughout the envelope, but rather may be steeper close to the dissipation region, where the gravitational potential increases abruptly. To quantify this, at least approximately, we follow Livio & Soker (1988) and estimate the parameter γ_{CE} defined by

$$\gamma_{\text{CE}} \equiv \frac{\tau_{\text{spin-up}}}{\tau_{\text{decay}}}, \quad (4)$$

where τ_{decay} represents the decay time-scale of the planet’s orbit, and $\tau_{\text{spin-up}}$ is the spin-up time-scale of the envelope. The decay time-scale is given by

$$\tau_{\text{decay}} = \left| \frac{a}{da/dt} \right| \approx \frac{G M_{\text{bd}} M(a)}{2a} \times \frac{1}{F_{\text{drag}} V}, \quad (5)$$

where $M(a)$ the mass interior to a , and F_{drag} is the gravitational drag force that causes the spiralling-in. Its expression is approximately given by

$$F_{\text{drag}} \approx \xi \pi R_a^2 \rho V^2, \quad (6)$$

where ξ is a factor of order 2–5 for supersonic flows (e.g. Shima et al. 1985), $R_a \approx 2GM/V^2$ is the accretion radius, V is the relative velocity between the planet and the envelope, and ρ is the local density. Finally, the spin-up time-scale $\tau_{\text{spin-up}}$ can be approximated by

$$\tau_{\text{spin-up}} = \frac{I(a)V}{a^2 F_{\text{drag}}}, \quad (7)$$

where $I(a)$ is the moment of inertia of the envelope interior to radius a . In the computations for our presented models, we assumed that the relative velocity V is Keplerian, and impose $\xi = 4$ as in Livio & Soker (1988). Fig. 8 depicts the profiles of γ_{CE} for the three initial models. Although these profiles are crude estimates, they suggest that a strong differential rotation is likely to take place at the base of the convective envelope, in the regions where $\gamma_{\text{CE}} < 1$. The shear can then sustain a dynamo action and lead to a high X-ray emission (e.g. Regos & Tout 1995). Furthermore, the profiles of γ_{CE} indicate that for less evolved configurations the outer layers are not spun up, and therefore that it is possible to obtain X-ray emission from apparently slowly rotating stars as observed among β Ceti-like stars. It is difficult to estimate for how long the slow rotation will be maintained at the surface of the star, since such a study would require to take into account the angular momentum transport in the convective envelope coupled with the presence of a strong magnetic field. Additionally, the outcome depends on the evolutionary status of the star. We expect, however, that the spin-up of the envelope will take longer in younger and less centrally condensed stars for which $\gamma_{\text{CE}} > 1$ in a larger fraction of the envelope. In some configurations magnetic braking may not allow a significant spin-up of the outer layers. Some indications that differential rotation may persist in the interior of stars are suggested by observations.

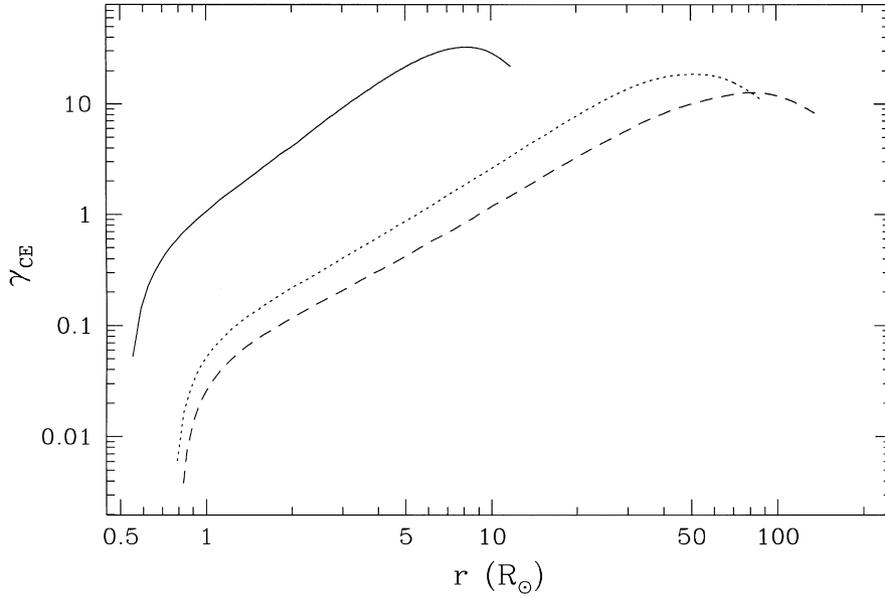


Figure 8. The parameters γ_{CE} as a function of the radius for the three initial models (see text). In the expression for τ_{decays} we took $M_{\text{bd}} = 10M_{\text{Jup}}$. The solid, dotted and dashed lines correspond to the initial models #A, #B and #C, respectively.

Indeed, in the HR diagram, the rotational (Section 4.2) and X-ray dividing lines are shifted with respect to one another. Thus stars located between these two lines present both a magnetic activity and a slow rotation rate. If this shift between the dividing lines corresponds effectively to an evolutionary sequence, this indicates either that the rotational braking time-scale is shorter than the decay time-scale associated with the dynamo activity or, alternatively, that differential rotation is still maintained in the stellar interior and sustains a dynamo activity.

To summarize this section, the deposition of angular momentum by a spiralling-in planet/brown dwarf can produce a strong differential rotation at the base of the convective envelope. We then suspect that in this region a magnetic field can be generated via an $\alpha-\Omega$ dynamo, and that this may ultimately result in an enhanced X-ray activity. Note that the magnetic field can also be used to brake the star. Finally, we would like to mention that the shear may trigger some instabilities that could give rise to extra mixing processes (see Section 4.6).

4.4 The ejection of shells

The increase in the mass-loss rate during the accretion phase can lead to the formation of a shell around the star, and that shell can be expected to emit in the infrared (IR). More quantitatively, the mass-loss rate can be increased by a factor of 2 to ~ 100 , and a mass of the order $10^{-6} M_{\odot} \lesssim M_{\text{eject}} \lesssim 10^{-3} M_{\odot}$ can be ejected. These numbers depend, however, on the evolutionary status of the star, the duration of the accretion event, and the accretion rate. Fig. 9 demonstrates the very strong dependence of the mass-loss rate on the accretion rate and on the initial model. The higher the accretion rate, the larger is the increase in the mass-loss rate. Similarly, the more evolved the star, i.e., the lower its surface gravity, the easier it is to remove material from its surface. Fig. 9 also indicates that the rate of increase in \dot{M}_{loss} is faster for older stars. This is an illustration of the thermal response of the star, since \dot{M}_{loss} is inversely proportional to the Kelvin–Helmholtz

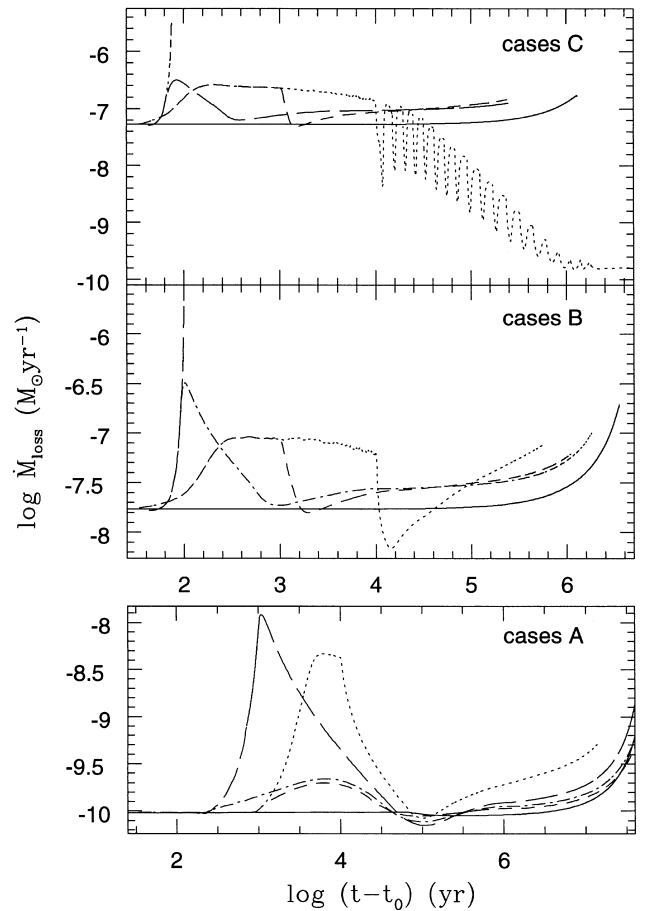


Figure 9. The evolution of the mass-loss rate is shown for our different models. The solid lines refer to the standard evolution. In the lower panel, the dotted, short-dashed, long-dashed and dot-dashed lines correspond to cases A0, A1, A2 and A3, respectively. The same lines refer to cases B0, B1, B2 and B3 in the middle panel, and to cases C0, C1, C2 and C4 in the upper panel, respectively. The peaks in \dot{M}_{loss} in the upper panel are due to thermal pulses.

time-scale ($\dot{M}_{\text{loss}} \propto M/\tau_{\text{KH}}$). Finally, we would like to emphasize that in the high accretion rate cases (cases B2 and C2), even a relatively small planet of a few Jupiter masses can increase the mass-loss rate by about 2 orders of magnitude in a few hundred years!

It is worth noting that in the estimates of the mass-loss rate, the effects of rotation have been neglected. The deposition of the orbital angular momentum into the envelope can lower the effective surface gravity and facilitate mass ejection; it can also influence of geometry of the ejection. In particular, if the rotational velocity of the star exceeds some fraction of the break-up speed, then the ejected material could form an equatorially compressed outflow (e.g. Bjorkman & Cassinelli 1993; Owocki, Cranmer & Blondin 1994; Livio 1997). The peculiar circumstellar environment of U Equulei could be consistent with such a scenario (Barnbaum et al. 1995).

The IR emission associated with giant stars is not easy to explain (Zuckerman, Kim & Liu 1995), while in main-sequence stars (Vega-like stars) the emission most likely arises from the dust associated with remnants of the star formation process or with small bodies like comets or planetesimals (e.g. Aumann et al. 1984; Telesco & Knacke 1991; Backman & Paresce 1993). In an extensive survey of luminosity class III stars, Plets et al. (1997) report that ~ 8 per cent of the giants in their sample have IR excesses. They conclude that the IR emission is unlikely to be due to a present-day mass-loss episode because, as they argue, (i) in a standard evolution, mass-loss is predominantly efficient during a He shell flash, so one would expect the stars to be more clustered at higher luminosities in the HR diagram, and (ii) the dust emission is too cold for a recent ejection. They thus attribute the IR excess to a reheated dusty disc, as in Vega-like stars. Instead, we propose that the ejection of a shell resulting from an accretion event can account for the IR emission. Indeed, this scenario does not imply a clustering of stars at the tip of the RGB, since the accretion event can, in principle, take place at any time after the star leaves the main-sequence. Early engulfing could also account for the cold dust emission. Moreover, the IR excess is often too large to be attributed to a Vega-like phenomenon, since during the main-sequence phase, most of the circumstellar debris will probably be evaporated (Zuckerman et al. 1995). An important test of our scenario can be provided by measuring the ${}^7\text{Li}$ abundance for example, since this element should, at some level, accompany the accretion process (see Section 4.6).

The detection of a detached shell around the J-type carbon star Y Canum Venaticorum (Izumiura et al. 1996) is also interesting, since this star is probably in an early evolutionary stage, on the RGB or on the He core-burning stage. The mass-loss rates at the time of shell formation and the mass of the shell are estimated to be in the ranges $(7\text{--}20) \times 10^{-6} M_{\odot} \text{ yr}^{-1}$ and $(4\text{--}10) \times 10^{-2} M_{\odot}$, respectively. The present mass-loss rate estimated from CO observations (e.g. Olofsson et al. 1993) is about $10^{-7} M_{\odot} \text{ yr}^{-1}$, two orders of magnitude smaller than the past value! Therefore, if the RGB status of Y CVn is confirmed, the existence of a massive shell around this star may be a signature of an accretion event, since no other straightforward model can account for these observations. In this context, the massive shell and high mass-loss rate at the time of ejection would suggest a very high accretion rate ($\dot{M}_{\text{acc}} \gtrsim 10^{-4} M_{\odot} \text{ yr}^{-1}$).

Shells have also been observed around many AGB stars (e.g. Olofsson et al. 1992, 1996; Bujarrabal & Cernicharo 1994), but such structures can result from episodic high mass-loss events triggered by helium shell flashes (e.g. Olofsson et al. 1990;

Izumiura et al. 1997). It is therefore difficult to identify the signature of an accretion event, although the presence of a companion is frequently invoked for the shaping of planetary nebulae (e.g. Livio 1997; Soker 1997). Finally, we should mention that in model C0 the star experiences a series of thermal pulses before reaching the horizontal branch. From the simulations we can estimate that during every interpulse, a mass of the order of $4 \times 10^{-4} M_{\odot}$ is ejected from the surface of the giant. These episodic ejections would generate distinct shells, separated from each other by a few thousand years. However, the probability that a massive planet would be engulfed at the short-lived tip of the giant branch is rather small.

4.5 Influence on the morphology of globular clusters

The distributions of stars along the horizontal branch (HB) of globular clusters varies from one cluster to another. In some clusters, the population of HB stars exhibits an extended blue tail, while others contain only a red HB. It was first recognized by Sandage & Whitney (1967) that the metallicity is the first parameter influencing the morphology of the HB. Generally, more metal-rich clusters have red HBs, while metal-poor clusters have bluer HBs. However, for globular clusters of the same metallicity, the HB morphology can vary widely. Thus some ‘second parameter’ other than metallicity must be affecting the HB morphology. Among potential second parameters, it has been shown that age (e.g. Lee, Demarque & Zinn 1994), mass-loss (e.g. D’Cruz et al. 1996), He mixing (Sweigart 1997), CNO enhancement (Dorman, Lee & Vandenberg 1991), core rotation, or structural properties of the globular clusters such as concentration and density can also affect the HB morphology. Nevertheless, the discovery of gaps in the blue tail of the HB (e.g. Walker 1992; Catelan et al. 1998; Ferraro et al. 1998) is still considered puzzling.

Recently, Soker (1999) suggested that planetary systems can influence the HB morphologies. He proposed that the interaction of a RGB star with a giant planet/brown dwarf can affect the mass-loss rate and thus the subsequent location of the star on the HB. By depositing angular momentum and energy into the envelope, additional mass can be removed from the star during the RGB. The ‘peeled off’ star will then have a higher effective temperature and will appear bluer in the HR diagram (e.g. Castellani & Castellani 1993; Dorman, Rood & O’Connell 1993). In particular, Soker (1999) argued that, depending on whether the planet survives the spiralling-in, collides with the stellar core, or evaporates in the envelope, one can account for the three gaps observed by Sosin et al. (1997) in the blue tail of NGC 2808.

Our study introduces a quantitative element into the scenario proposed by Soker. Our computations indeed indicate that a significant increase in the mass-loss rate accompanies the accretion process, especially if the star is evolved and the accretion rate is high. The simulations also show that, when the star has relaxed, the mass-loss rate remains higher than in a standard evolution. We estimated that when a massive planet is accreted (not a brown dwarf), the mass-loss rate is enhanced by a factor of 1.3–2 after the termination of the accretion process. This is equivalent to setting Reimer’s parameter η_R to a value close to 0.7–1.0 (instead of 0.5) in a standard evolution. If we now refer to the computations of Castellani & Castellani (1993) for such values for η_R , we conclude that stars accreting a planet at the bottom of the RGB will actually be extremely blue on the horizontal branch.

On the other hand, if the accretion occurs later, the effects are difficult to quantify because of the strong sensitivity of our computations to the accretion rate and the planet mass. The effects can be moderate, as in cases C2 or B2, or dramatic, as in cases B3 or C4. The possibility that a planet accretion would modify the evolutionary age of the star and thus affect the morphology of the HB is improbable. Indeed, our initial models are relatively old ($t_0 > 12$ Myr), and the duration of the red giant phase is relatively short compared to its age. Also, the accretion of a planet does not modify substantially the mass of the star; therefore we do not expect the stellar evolutionary time-scales to be significantly modified.

Sweigart (1997) suggested that an extra mixing driven by internal rotation could transport helium from the HBS into the convective envelope. This would increase the RGB tip luminosity and hence the mass-loss, leading to the formation of blue HB stars. Sweigart & Catelan (1998) also showed that *only* non-canonical mechanisms invoking deep helium mixing, internal rotation or a high initial helium abundance can reproduce the distribution of the blue HB stars in NGC 6388 and 6441. However, these authors did not specify the source of the angular momentum required for the rotation scenario nor how the deep He-mixing process is activated. The accretion scenario can provide some support for these non-canonical processes, since it both offers a natural source of angular momentum for the core and can be responsible for the generation of strong instabilities as the planet collides with the core (Section 4.3). Note also that some rapid rotators are observed in the blue side of the HB (e.g. Harris & McClure 1985).

Concerning the gaps, recent observations (Ferraro et al. 1998) indicate that they are not randomly distributed along the HB, but rather located at similar positions in the colour–magnitude diagram. Aside from the star–planet interaction hypothesis (Soker 1999), it has been suggested that some poorly specified physical processes must operate during the RGB to increase the mass-loss rate (Ferraro et al. 1998), or that gaps are a consequence of a bimodal or multimodal mass distribution of the globular clusters (e.g. Catelan et al. 1998). Let us therefore return to the planet accretion scenario and analyse the implications of this assumption. We have seen that, depending on the evolutionary status of the star at the time of engulfing (i.e., on the initial planet separation), different amounts of mass can be lost and thus different positions in the HB can be reached. Assuming for the moment that planets form preferentially around solar-type stars (as has been observed so far), the similarity in the positions of the gaps would suggest that planets orbit at preferred distances to the star. A theory suggesting that this is indeed the case exists (Nottale 1996; Nottale, Schumacher & Gay 1997, and references therein). If this is true, planets would be swallowed only when the solar-type star reaches a certain radius (or equivalently an evolutionary status), determined approximatively by the orbital separation of the planet. In this hypothesis, the accretion process would modify selectively the mass-loss rate and thus the location of the star on the HB.

However, the question of why the star–planet interaction process acts only sporadically and does not appear as a general phenomenon affecting the morphology of all the clusters would remain puzzling. To attempt to answer this question, one needs a better understanding of the processes involved in planetary formation. For example, metallicity and other globular cluster properties such as density may be important factors that can influence the formation of planets, and they are still poorly

understood. To conclude this section, the accretion of planets by giant stars can potentially influence the mass-loss rate and thus modify the position of the star on the HB. However, it is not clear at present that the gaps observed in the blue tail of some globular clusters are really the signature of such accretion events.

4.6 The lithium-rich G and K giants

The detection of lithium in the spectra of G and K giants (e.g. Wallerstein & Sneden 1982; Brown et al. 1989; Gratton & D’Antona 1989; Pilachowski, Sneden & Hudek 1990; Castilho, Barbuy & Gregorio-Hetem 1995; de la Reza & da Silva 1995; Castilho et al. 1998) poses a problem concerning the origin of this element in these stars since, in standard evolution, lithium is entirely depleted during the first dredge-up. Several mechanisms have been suggested to explain the Li enrichment, and we refer to Gratton & D’Antona (1989) for a more complete discussion. Briefly, it has been proposed, for example, that Li could be preserved in the atmosphere of giant stars, but the low $^{12}\text{C}/^{13}\text{C}$ ratio observed in these stars (e.g. Pilachowski et al. 1990; de la Reza, da Silva & Barbuy 1995) indicates that deep mixing (and thus Li burning) has occurred. This represents therefore a failure of this scenario. Gratton & D’Antona considered the possibility that the giant’s envelope could be contaminated by a nova exploding companion. However, the non-detection of a white dwarf in the vicinity of Li-rich giants (e.g. de la Reza & da Silva 1995) weakens this hypothesis. The possibility that Li could be produced by the Cameron–Fowler mechanism (1971) has also been investigated. This mechanism, which consists of the rapid dredge-up of ^7Be and Li production through the $^7\text{Be}(e^-, \nu)^7\text{Li}$ reaction, is known to operate in AGB stars of 4–6 M_{\odot} for which the convective time-scale is short compared to the ^7Be destruction time-scale (Sackmann & Boothroyd 1992). Unfortunately, this process is inefficient in low-luminosity stars, unless one invokes some extra mixing processes (we will return to this point later). Finally, and we will develop this point below, several authors (e.g. Alexander 1967; Brown et al. 1989; Gratton and D’Antona 1989) proposed that the engulfing of a planet or a brown dwarf could be responsible for the high Li abundance.

Based on *IRAS* observations of G and K giants, de la Reza et al. (1996, 1997) concluded that *almost all* the Li-rich G and K giants have an IR excess compatible with the presence of a circumstellar shell. To account for these observations, they constructed a model in which Li is produced inside the star by an extra mixing process, the ‘cool bottom burning’ (Wasserburg, Boothroyd, Sackmann 1995). This process allows the fast transport of ^7Be from the HBS into the convective envelope, where ^7Be then decays to produce ^7Li . Furthermore, they assumed that the mechanism for Li enrichment is accompanied by a sudden increase in the mass-loss rate and thereby the ejection of a shell. Following the evolution of a thin expanding circumstellar shell, they could reasonably account for the IR emission and Li abundance distribution of G and K giants in a colour–colour diagram. However, de la Reza et al. remained relatively vague concerning the mechanism that is responsible for mass-loss; they assumed that it is a consequence of the Li enrichment process. Instead, we propose here that the accretion of a planet or a brown dwarf can naturally and consistently explain all of the observed features. We describe our scenario in the next paragraph and illustrate it in Fig. 10, which is an adaptation of fig. 2 of de la Reza et al. (1996).

Fig. 10 represents a colour–colour diagram based on the *IRAS*

Possible scenario for the formation of IR excess and high Li abundance

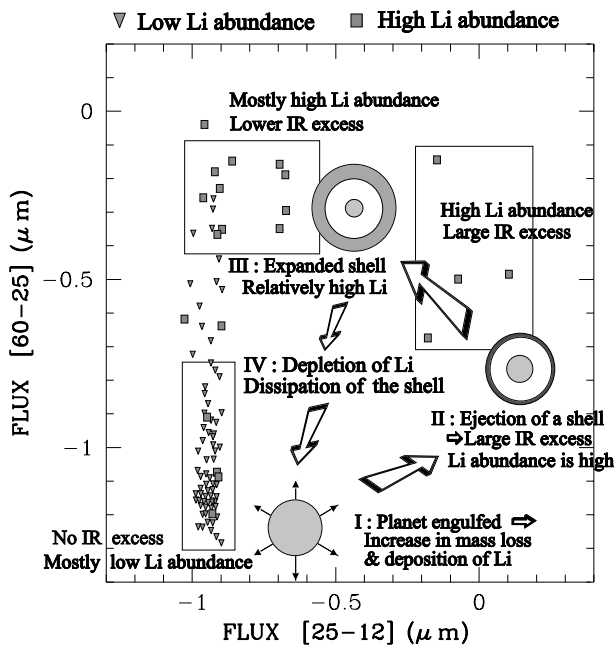


Figure 10. The schematic evolution in an *IRAS* colour–colour diagram of a K giant star engulfing a planet or a brown dwarf. (By definition, $[\lambda_1 - \lambda_2] = \log \lambda_2 S_{\lambda_1} - \log \lambda_1 S_{\lambda_2}$, where S_{λ} is the *IRAS* density flux.) This figure was adapted from de la Reza et al. (1996), and is explained in the text.

density fluxes at 12, 25 and 60 μm . In this diagram, de la Reza et al. (1996, hereafter DDD) identified three regions, populated respectively by normal K giants with no IR excess (region *I*), Li-rich giants with a large IR excess (region *II*), and relatively Li-rich giants with a moderate IR excess (region *III*). When the accretion process starts, Li is progressively deposited in the stellar envelope and the mass-loss rate increases. Rapidly, a shell is ejected and the giant moves quickly from region *I* to region *II*. In their shell model, DDD found that several hundred years are required to reach region *II*. This time-scale gives an estimate of the duration of the accretion process. Then, Li starts to be depleted in the envelope, while the shell expands and cools down. The 25- μm flux decreases and the star now settles in region *III*. DDD estimated that it takes approximately 10^4 yr to move from region *II* to *III*. Finally, in about 8×10^4 yr, the circumstellar shell dissipates, Li is entirely depleted, and the star returns to region *I* as a normal K giant. Assuming a wind velocity of 2 km s^{-1} and a mass-loss rate of $5 \times 10^{-8} M_{\odot} \text{ yr}^{-1}$, DDD found that $\sim 10^{-5} M_{\odot}$ was ejected in the shell, in agreement with our models. In a second publication, de la Reza et al. (1997) completed their study by presenting new observations. They showed that Li-rich and Li-poor stars are mixed in the colour–colour diagram. They interpreted these observations as being due to differences in the Li destruction time-scales. In our model, this is explained naturally if the amount of Li deposited into the star, or equivalently the mass of the planet, is different from one star to another.

The mechanism that leads to the Li enrichment must also account for its rapid depletion, which takes place in $\sim 10^5$ yr. In our computations without diffusion, Li is maintained at the surface of the star, but Charbonnel (1995) showed that this element can be

rapidly depleted in red giants due to non-standard mixing processes. In particular, the model developed by Zahn (1992) showed that the efficiency of the mixing is mainly determined by the loss of angular momentum via a stellar wind and, even in the absence of a high mass-loss rate, the process takes place where there is a strong gradient in ω . He also pointed out that additional mixing is expected in shell-burning regions. Since all of these conditions are satisfied in the context of the accretion process (increase in the mass-loss rate, deposition of angular momentum, and a strong gradient of ω in the dissipation region as described in Section 4.3), and as a part of the fact that the star is on the RGB (the presence of the HBS), we have every reason to believe that the mechanism proposed by Zahn (1992), which successfully explains some peculiar anomalies in red giant stars (Charbonnel 1995), could be responsible for the fast Li depletion following a short accretion phase. Moreover, observations of the $^{12}\text{C}/^{13}\text{C}$ ratio in some Li-rich giants (de la Reza & da Silva 1995) indicate that some extra mixing is operating, since the carbon isotope ratio in these stars is lower than the standard value. Our scenario does encounter some difficulties in explaining the very high Li abundances [$\log \epsilon(\text{Li}) \geq 2.8$] found in some giants (e.g. Gratton & D’Antona 1989; de la Reza & da Silva 1995; Fekel et al. 1996). This would require the deposition of a huge amount of lithium that can only be achieved either by the accretion of numerous planets such that $M_{\text{acc}} \approx M_{\text{env}}$, or if the Li abundance in the brown dwarf is extremely high ($X^{\text{acc}} \geq 10 \times X^{\text{env}}$ for $M_{\text{acc}} \approx 0.1 M_{\odot}$). The accretion scenario does not provide a straightforward explanation, but we can imagine that when the planet reaches the central region, the dissipation process may generate some instabilities (due to the shear) that could, in turn, trigger the ‘cool bottom burning’ invoked by de la Reza et al. (1996, 1997). The accretion process would then lead to some Li production (as in more massive AGB stars).

De Medeiros et al. (1996a) reported that the majority of Li K giants are normal rotators ($v \sin i \approx 2\text{--}3 \text{ km s}^{-1}$), although some exceptions exist [e.g. HD 233517 (Fekel et al. 1996), HD 9746, 25893, 31993, 33798 and 203251 (Fekel & Balachandran 1993), and 1E 1751+7046 (Ambruster et al. 1997)]. However, as pointed out in Section 4.2, high angular velocities (~ 10 per cent per cent of the Keplerian velocity) can be achieved only if a sufficiently massive planet ($M_{\text{bd}} > 5M_{\text{Jup}}$) is accreted. For a typical $1.0 M_{\odot}$ RGB star, with a radius $R \sim 20R_{\odot}$, the deposition of the orbital angular momentum of a $5M_{\text{Jup}}$ planet will ‘only’ increase the star’s rotational velocity to $\sim 5.5 \text{ km s}^{-1}$ (equation 3). Consequently, as long as the mass of the engulfed body is low (a planet rather than a brown dwarf), the observed angular momentum of Li-rich giants is compatible with our scenario. We should also note that due to the increased mass-loss, magnetic braking could also be operating (e.g. Leonard & Livio 1995). Finally, let us point out that *all the Li-rich giants are single stars*, and so, according to the prevailing common wisdom, they could possess planetary systems.

To summarize this section, we propose that the accretion of a planet or a brown dwarf is responsible for both the IR excess and the high Li abundance present in almost all single Li-rich G and K giants.

5 DISCUSSION AND CONCLUSIONS

In this paper we investigated the effects of the accretion of a planet or a brown dwarf by a solar-type star located on the red giant

branch. Our computations show that the deposition of mass (potential energy) produces a substantial expansion of the envelope and, for higher accretion rates, nuclear burning at the base of the convective envelope can take place. The simulations show that the results are a sensitive function of the accretion rate and the structure of the star. Generally, the higher the accretion rate and/or the more evolved the star, the larger is the expansion. After the end of the accretion process, the star relaxes and resumes a standard evolution. However, in one simulation (case C0), the star avoided the He flash, but instead developed thermal instabilities. For this model, after a phase of thermal pulses, He burning was finally ignited at the centre of the star.

We discussed the possible observational signatures of the accretion of a planet/brown dwarf as follows. (1) We showed that the rotational velocity of the star can be substantially increased, provided that the accreted planet/brown dwarf is sufficiently massive. In this respect the accretion of a brown dwarf could account for the fast rotation of FK Comae stars and, more generally, the deposition of angular momentum via this process can explain unusually fast rotation rates. (2) Investigating the X-ray properties of giant stars, we showed that a strong differential rotation may take place at the bottom of the convective envelope. The presence of shear in this region can turn on the dynamo activity, and this may ultimately generate X-ray emission. We showed that under some conditions the surface layers of the star could rotate slowly, while a rapid rotation is maintained in the core. (3) We also showed that the accretion scenario can lead to the ejection of shells whose mass is in the range $10^{-6} M_{\odot} \lesssim M_{\text{eject}} \lesssim 10^{-3} M_{\odot}$. The IR excesses observed in ≈ 8 per cent of luminosity class III stars could in part be due to this process. (4) We argued that the increase in the mass-loss rate can also have indirect effects on the morphology of the horizontal branch, and in this respect the accretion process is a potential second-parameter candidate. (5) We showed that the deposition of planet material in the convective envelope can efficiently increase the ${}^7\text{Li}$ surface abundance and, more generally, enhance the stellar metallicity of giant stars. (6) Finally, on a related topic, we proposed that the accretion of a planet/brown dwarf can explain consistently both the IR excess and the high Li abundance observed only in single red giant stars.

In terms of physical processes, we suggested that planet/brown dwarf accretion may provide the triggering for a variety of processes. For example, the disruption of the planet and the associated instabilities could increase the He abundance in the giant's envelope and thus affect the morphology of the HB, as proposed by Sweigart (1997, see our Section 4.5). They could also be responsible for the production of lithium through the mechanism proposed by Wasserburg et al. (1995; see our Section 4.6). Finally, the rapid contraction of the star at the end of the accretion process could generate some pulsations.

Observations indicate that several of potential different signatures of an accretion event, e.g., a fast rotation rate, a significant X-ray emission, a high Li abundance or a large IR excess, do not always occur simultaneously. As we have shown, this is not surprising. First, depending on the mass of the planet, the outcomes could be different. For example, a small planet that evaporates in the envelope before reaching its base will perturb the structure only slightly. In such a case, no shell will be ejected, but the deposition of angular momentum and matter in the surface layers could still produce a relatively rapid rotation and a high Li abundance, as observed in some chromospherically active giants (Fekel & Balachandran 1993). Secondly, the time-scales associated with the various phenomena (IR excess, X-ray activity,

rotational braking, particle transport) can be different, and thus not all the signatures will be observed at the same time. For example, if the spin-down time-scale is longer than the time-scale associated with the dissipation of the ejected shell, one can account for the absence of IR excess in some fast rotators. Thirdly, the consequences of the accretion process depend on the evolutionary status of the star. Giant stars located at the bottom of the RGB have much deeper convective envelopes than near the tip of the giant branch. Thus, if we consider, for example, the deposition of Li in the envelope, it is more difficult to obtain high Li abundances in younger red giants (it is also more difficult to eject a shell). Finally, our simulations show that the results are sensitive to the physics of the dissipation process and, more specifically, to the accretion rate and the location of the accretion process. At present, both these physical parameters are rather uncertain, and a better understanding of the dissipation process is definitely required.

As a last point, we can attempt to use the expected observational signatures to infer some estimate for the frequency of planets around solar-type stars. In a search for lithium in 644 G and K giants, Brown et al. (1989) found that 2 per cent of the stars of their sample have $\log \epsilon(\text{Li}) \geq 1.5$ and 4 per cent have $\log \epsilon(\text{Li}) > 1.3$. If we adopt for our definition of Li-rich giants the value $\log \epsilon(\text{Li}) > 1.2$, we find that ~ 8 per cent of the stars surveyed by Brown et al. belong to this group. In a more recent survey, Castilho et al. (1998) report the detection of five Li-rich and six moderately Li-rich giants among 164 stars, indicating a proportion of Li-rich giants of ~ 3 –7 per cent. The study of Plets et al. (1997) indicates that 8 per cent of luminosity class III giants have unexpected IR excess. Finally, based on rotational velocity measurements of ~ 900 G and K giants, De Medeiros et al. (1996a) found that ≈ 5 per cent of late G and K giants located beyond the rotational dividing line are fast rotators with $v \sin i > 5 \text{ km s}^{-1}$. Thus, if the IR excess and/or high Li abundance and/or unusually high rotational velocity among G and K giants result from the accretion of a planet/brown dwarf, the above numbers suggest that at least 4–8 per cent of the single, solar-type stars must have a low-mass companion, either a brown dwarf or a planet. If we were to take seriously the frequency of planets inferred by Soker (1997) to account for the shaping of planetary nebulae (~ 55 per cent of all progenitors of masses $\leq 5 M_{\odot}$), our deduced frequency would indicate that either a large fraction of the planets do not interact during the red giant phase or, more probably, that the observational signatures of the accretion event are very short-lived compared to stellar evolutionary time-scales. Indeed, because of the large radii reached by solar-type stars during the RGB, some planets will most likely be engulfed during the early giant phase rather than on the AGB (although Jupiter will not be engulfed by our own Sun). On the other hand, if we compare the time-scales associated with both the Li and IR excesses ($\geq 10^5$ yr) to the red giant lifetime (between 6×10^6 and 5×10^8 yr for giants with masses between 1.0 and $2.5 M_{\odot}$), we conclude that the probability of detecting an accretion event is such that we are likely to miss most candidates.

ACKNOWLEDGMENTS

LS acknowledges support from the Director's Discretionary Research Fund at STScI, and thanks the STScI for its hospitality. This work has been supported in part by NASA grants NAGW-2678, G005.52200 and G005.44000. The computations presented

in this paper were performed at the ‘Centre Intensif de Calcul de l’Observatoire de Grenoble’.

REFERENCES

- Alexander J. B., 1967, *Observatory*, 87, 238
- Ambruster C. W., Fekel F. C., Guinan E. F., Hrivnak B. J., 1997, *ApJ*, 479, 960
- Anders E., Grevesse N., 1989, *Geochim. Cosmochim. Acta*, 53, 197
- Aumann H. H. et al., 1984, *ApJ*, 278, L23
- Ayres T. R., Simon T., Stern R. A., Drake S. A., Wood B., Brown A., 1998, *ApJ*, 496, 428
- Backman D. E., Paresce F., 1993, in Levy E. H., Lunine J. I., eds, *Protostars and Planets III*. Univ. Arizona Press, p. 1253
- Barnbaum C., Morris M., Kahane C., 1995, *ApJ*, 450, 862
- Basri G., Marcy G. W., Graham J. R., 1996, *ApJ*, 458, 600
- Bjorkman J. E., Cassinelli J. P., 1993, *ApJ*, 409, 429
- Bopp B. W., Stencel R. E., 1981, *ApJ*, 247, L131
- Brown J. A., Sneden C., Lambert D. L., Dutchover E. Jr., 1989, *ApJS*, 71, 293
- Bujarrabal V., Cernicharo J., 1994, *A&A*, 288, 551
- Butler R. P., Marcy G. W., 1996, *ApJ*, 464, L153
- Butler R. P., Marcy G. W., Vogt S. S., Apps K., 1998, *PASP*, 110, 1389
- Cameron A. G. W., Fowler W. A., 1971, *ApJ*, 164, 11
- Castellani M., Castellani V., 1993, *ApJ*, 407, 649
- Castilho B. V., Barbuy B., Gregorio-Hetem J., 1995, *A&A*, 297, 503
- Castilho B. V., Gregorio-Hetem J., Spite F., Spite M., Barbuy B., 1998, *A&AS*, 127, 139
- Catelan M., Borissova J., Sweigart A. V., Spassova N., 1998, *ApJ*, 494, 265
- Charbonnel C., 1995, *ApJ*, 453, L41
- Cochran W. D., Hatzes A., Marcy G. W., Butler R. P., 1997, *ApJ*, 483, 457
- Cohen J. G., McCarthy J. K., 1997, *AJ*, 113, 1353
- D’Cruz N. L., Dorman B., Rood R. T., O’Connell R. W., 1996, *ApJ*, 466, 359
- Delfosse X., Forveille T., Mayor M., Perrier C., Naef D., Queloz D., 1998, *A&A*, 331, 581
- de la Reza R., da Silva L., 1995, *ApJ*, 439, 917
- de la Reza R., da Silva L., Barbuy B., 1995, *ApJ*, 448, L41
- de la Reza R., Drake N. A., da Silva L., 1996, *ApJ*, 456, L115 (DDD)
- de la Reza R., Drake N. A., da Silva L., Torres C. A. O., Martin E. L., 1997, *ApJ*, 482, L77
- de Medeiros J. R., Melo C. H. F., Mayor M., 1996a, *A&A*, 309, 465
- de Medeiros J. R., da Rocha C., Mayor M., 1996b, *A&A*, 314, 499
- Dorman B., Lee Y. W., VandenBerg D. A., 1991, *ApJ*, 366, 115
- Dorman B., Rood R. T., O’Connell R. W., 1993, *ApJ*, 419, 596
- Fekel F. C., 1988, in Rolfe E. J., ed., *Decade of UV Astronomy with IUE Satellite*. ESA Publications, Noordwijk, The Netherlands, Vol. 1, p. 331
- Fekel F. C., Balachandran S., 1993, *ApJ*, 403, 708
- Fekel F. C., Marschall L. A., 1991, *AJ*, 102, 1439
- Fekel F. C., Webb R. A., White R. J., Zuckerman B., 1996, *ApJ*, 462, L95
- Ferraro F. R., Paltrinieri B., Fusi Peci F., Rood R. T., Dorman B., 1998, *ApJ*, 500, 311
- Forestini M., Charbonnel C., 1997, *A&AS*, 123, 241
- Gonzalez G., 1997, *MNRAS*, 285, 403
- Gonzalez G., 1998, *A&A*, 334, 221
- Gratton R. G., D’Antona F., 1989, *A&A*, 215, 66
- Gray D. F., 1981, *ApJ*, 251, 155
- Gray D. F., 1982, *ApJ*, 262, 682
- Gray D. F., 1986, *Highlights Astron.*, 7, 411
- Gray D. F., 1989, *ApJ*, 347, 1021
- Gray D. F., 1991, in Catalano, S., Stauffer J. R., eds, *Angular Momentum Evolution of Young Stars*. Kluwer, Dordrecht, p. 183
- Gray D. F., Nagar P., 1985, *ApJ*, 298, 756
- Haisch B., Schmitt J. H. M. M., Rosso A. C., 1991, *ApJ*, 383, L15
- Haisch B., Schmitt J. H. M. M., Fabian A. C., 1992, *Nat*, 360, 239
- Harpaz A., Soker N., 1994, *MNRAS*, 270, 734
- Harris H. C., McClure R. D., 1985, *PASP*, 97, 261
- Hünsch M., Schröder K.-P., 1996, *A&A*, 309, L51
- Hünsch M., Schmitt J. H. M. M., Schröder K. P., Reimers D., 1996, *A&A*, 310, 801
- Hünsch M., Schmitt J. H. M. M., Schröder K. P., Zickgraf F. J., 1998, *A&A*, 330, 225
- Iben I. Jr., Livio M., 1993, *PASP*, 105, 1373
- Izumiura H., Hashimoto O., Kawara K., Yamamura I., Waters L. B. F. M., 1996, *A&A*, 315, L221
- Izumiura H., Waters L. B. F. M., de Jong T., Loup C., Bontekoe Tj. R., Kester D. J. M., 1997, *A&A*, 323, 449
- Kraft R. P., 1970, in Herbig G. H., ed., *Spectroscopic Astrophysics*. Univ. California Press, Berkeley, p. 385
- Laughlin G., Adams F. C., 1997, *ApJ*, 491, L51
- Lee Y. W., Demarque P., Zinn R., 1994, *ApJ*, 423, 248
- Leonard P. T. J., Livio M., 1995, *ApJ*, 447, L21
- Lin D. N., Bodenheimer P., Richardson D. C., 1996, *Nat*, 380, 606
- Livio M., 1997, *Space Sci. Rev.*, 82, 389
- Livio M., Soker N., 1984, *MNRAS*, 208, 763
- Livio M., Soker N., 1988, *ApJ*, 329, 764
- Maggio A., Favata F., Peres G., Sciortino S., 1998, *A&A*, 330, 139
- Marcy G. W., Butler R. P., Vogt S. S., Fischer D., Lissauer J. J., 1998, *ApJ*, 505, L147
- Mayor M., Queloz D., 1995, *Nat*, 378, 355
- Nottale L., 1996, *A&A*, 315, L9
- Nottale L., Schumacher G., Gay J., 1997, *A&A*, 322, 1018
- Olofsson H., Carlström U., Eriksson K., Gustafsson B., Willson L. A., 1990, *A&A*, 230, L13
- Olofsson H., Carlström U., Eriksson K., Gustafsson B., 1992, *A&A*, 253, L17
- Olofsson H., Eriksson K., Gustafsson B., Carlström U., 1993, *ApJS*, 87, 267
- Olofsson H., Bergman P., Eriksson K., Gustafsson B., 1996, *A&A*, 311, 587
- Owocki S. P., Cranmer S. R., Blondin J. M., 1994, *ApJ*, 424, 887
- Peterson R. C., Tarbell T. D., Carney B. W., 1983, *ApJ*, 265, 972
- Peterson R. C., Rood R. T., Crocker D. A., 1995, *ApJ*, 453, 214
- Pilachowski C. A., Sneden C., Hudek D., 1990, *AJ*, 99, 1225
- Plets H., Waelkens C., Oudmaijer R. D., Waters L. B. F. M., 1997, *A&A*, 323, 513
- Rasio F. A., Tout C. A., Lubow S. H., Livio M., 1996, *ApJ*, 470, 1187
- Rebolo R., Zapatero-Osorio M. R., Martin E. L., 1995, *Nat*, 377, 129
- Rebolo R., Martin E. L., Basri G., Marcy G., Zapatero-Osorio M. R., 1996, *ApJ*, 469, L53
- Regos E., Tout C. A., 1995, *MNRAS*, 273, 146
- Reimers D., 1975, *Men. Soc. Roy. Sci. Liège*, 6th Ser. 8, 369
- Reimers D., Hünsch M., Schmitt J. H. M. M., Toussaint F., 1996, *A&A*, 310, 813
- Rosner R., An C. H., Musielak Z. E., Moore R. L., Suess S. T., 1991, *ApJ*, 372, L91
- Rosner R., Musielak Z. E., Cattaneo F., Moore R. L., Suess S. T., 1995, *ApJ*, 442, L25
- Rucinski S. M., 1985, *MNRAS*, 215, 591
- Rucinski S. M., 1990, *PASP*, 102, 306
- Sackmann I. J., Boothroyd A. I., 1992, *ApJ*, 392, L71
- Sandage A. R., Willey R., 1967, *ApJ*, 150, 469
- Sandquist E., Taam R. E., Lin D. N. C., Burkert A., 1998, *ApJ*, 506, L65
- Shima E., Matsuda T., Takeda H., Sawada K., 1985, *MNRAS*, 217, 367
- Siess L., Livio M., 1999, *MNRAS*, 304, 925
- Siess L., Forestini M., Bertout C., 1997, *A&A*, 326, 1001
- Simon T., Drake S. A., 1989, *ApJ*, 346, 303
- Soker N., 1997, *ApJS*, 112, 487
- Soker N., 1998, *ApJ*, 498, 833
- Soker N., 1999, in the *Proceedings of the 10th Cambridge Workshop on Cool Stars, Stellar Systems and the Sun*, in press
- Soker N., Harpaz A., Livio M., 1984, *MNRAS*, 210, 189
- Sosin C. et al., 1997, *ApJ*, 480, L35
- Stepien K., 1993, *ApJ*, 416, 368

- Strassmeier K. G., Hall D. S., Barksdale W. S., Jusick A. T., Gregory W. H., 1990, *ApJ*, 350, 367
- Strassmeier K. G., Handler G., Paunzen E., Rauth M., 1994, *A&A*, 281, 855
- Sweigart A. V., 1997, *ApJ*, 474, L23
- Sweigart A. V., Catelan M., 1998, *ApJ*, 501, L63
- Telesco C. M., Knacke R. F., 1991, *ApJ*, 372, L29
- Vitenbroek H., Dupree A. K., Gilliland R. L., 1998, *AJ*, 116, 2501
- Walker A. R., 1992, *PASP*, 104, 1063
- Wallerstein G., Sneden C., 1982, *ApJ*, 255, 577
- Wasserburg G. J., Boothroyd A. I., Sackmann I. J., 1995, *ApJ*, 447, L37
- Webbink R. F., 1977, *ApJ*, 211, 486
- Welty A. D., Ramsey L. W., 1994, *ApJ*, 435, 848
- Zahn J. P., 1992, *A&A*, 265, 115
- Zuckerman B., Kim S. S., Liu T., 1995, *ApJ*, 446, L79

This paper has been typeset from a $\text{\TeX}/\text{\LaTeX}$ file prepared by the author.